

Effective Hamiltonian model for helically constrained quantum systems within adiabatic perturbation theory: application to the Chirality-Induced Spin Selectivity (CISS) Effect

Matthias Geyer,^{1, a)} Rafael Gutierrez,^{1, b)} and Gianaurelio Cuniberti^{1, c)}

*Institute for Materials Science and Max Bergmann Center of Biomaterials,
TU Dresden, 01062 Dresden, Germany*

(Dated: 18 February 2022)

The chirality-induced spin selectivity (CISS) effect has been confirmed experimentally for a large class of organic molecules. Adequately modeling the effect remains a challenging task, with both phenomenological models and first-principle simulations yielding inconclusive results. Building upon a previously presented model by K. Michaeli and R. Naaman (J. Phys. Chem C 123, 17043 (2019)) we systematically investigate an effective 1-dimensional model derived as the limit of a 3-dimensional quantum system with strong confinement and including spin-orbit coupling. Having a simple analytic structure, such models can be considered a minimal setup for the description of spin-dependent effects. We use adiabatic perturbation theory to provide a mathematically sound approximation procedure applicable to a large class of spin-dependent continuum models. We take advantage of the models simplicity by analyzing its structure to gain a better understanding how the occurrence and magnitude of spin polarization effects relate to the model's parameters and geometry.

^{a)}e-mail: matthias.geyer@tu-dresden.de; Dresden Center for Computational Materials Science (DCMS), TU Dresden, 01062 Dresden, Germany

^{b)}e-mail: rafael.gutierrez@tu-dresden.de

^{c)}e-mail: gianaurelio.cuniberti@tu-dresden.de; Dresden Center for Computational Materials Science (DCMS), TU Dresden, 01062 Dresden, Germany

I. INTRODUCTION

Spin-selective transfer processes related to chiral symmetries of molecular systems have increasingly attracted the attention over the past few years.¹⁻¹⁴ The effect, which has been termed Chirality-Induced Spin-Selectivity (CISS), had already been experimentally demonstrated by Ray et al.¹⁵ as early as 1999, but a real breakthrough took place with the two experimental studies by Göhler et al.¹⁶ and Xie et al.¹⁷, using photoemission and AFM-based electrical transport probes, respectively. Meanwhile it seems well confirmed that the CISS effect is a generic feature of molecular systems displaying helical symmetry, although a fully consistent theoretical description is still needed.¹⁸⁻³⁸ The vast majority of theoretical models proposed so far assume a close connection between chirality and spin-orbit interactions in the molecular systems, a result which seems to be supported by recent DFT-based calculations.^{39,40} However, part of the focus has been shifted recently to a more detailed treatment of interface effects, which may play a non-trivial role,³⁶ as well as on correlation effects.³⁸

Although most of the theoretical approaches are based on tight-binding formulations, few of them started from a continuum formulation of the problem.^{18,22,28,37} When starting with a continuum model, it is common to simplify it by restricting the electron's movement to a curved path and thus reducing its spatial degrees of freedom to one, either by using a quantized version of the classical Hamilton function for a particle moving on a curve²⁸, or by assuming an infinitely strong confinement potential transversal to the helical path, leading to an exactly 1-dimensional effective Hamiltonian.²² In contrast, in Ref.³⁷ the exact eigenfunctions of an assumed transverse harmonic potential were used in order to approximately map the 3D Hamiltonian onto an effective 1D Hamiltonian (including an effective spin-orbit coupling). These transverse energy eigenstates (spinors) were labelled with an angular momentum index, thus keeping part of the 3D nature of the model. The resulting effective Hamiltonian, while providing a simple connection between geometry and spin-dependence, had some issues, such as the presence of terms proportional to an inverse power of the confinement length scale. This would imply arbitrarily large (spin-orbit) coupling constants.

The quantization approach²⁸ has the advantage that no confinement or projection is needed since the classical motion is already restricted to the curve via holonomic constraints. However, it is, from a formal mathematical point of view, not unambiguous⁴¹ and the relation of

the resulting description to the physics in the ambient 3-dimensional space is not very clear. Provided a well-defined limiting procedure exists, the approach based on a finite transversal confinement does not suffer from these problems. It is known that the effective Hamiltonian does depend on extrinsic properties of the curve (or more generally, the submanifold), i. e. its embedding into the ambient space⁴² and thus cannot be obtained by intrinsic quantization. This also means that the confined system will retain some information about its surroundings.

Starting with the work of da Costa⁴², adiabatic approximations of constrained quantum systems have been studied both in theoretical^{43,44} and mathematical physics⁴⁵. These results have been generalized for potentials varying arbitrarily along the submanifold,⁴⁶ using the concept of adiabatic perturbation theory.⁴⁷⁻⁵⁰ The works cited so far in this paragraph are all concerned with Schrödinger operators, consisting only of a kinetic and a potential energy term. In order to model spin-dependent processes in the absence of external magnetic fields, we need to include spin-orbit interactions, which make decomposing the Hamiltonian into a longitudinal (or tangent) and a transversal (or normal) contribution more complicated. An approximation scheme similar to da Costa's has been applied to systems including magnetic fields and spin-orbit coupling.⁵¹⁻⁵⁴ However, an in-depth investigation concerning the applicability of this procedure in the presence of spin-orbit coupling is still missing.

Taking as starting point and motivation the study of Ref.³⁷, we exploit the approach presented by Wachsmuth et. al.⁴⁶ to show that an adiabatic approximation is still possible for an electron confined to a helix in the presence of spin-orbit coupling, and calculate the effective Hamiltonian for different field configurations. Contrary to Ref.³⁷, where the spin-orbit interaction arose from the transversal confinement field, we consider a separate electric field as the source of spin-orbit coupling which is different from the confinement. We lay our focus on fields radially symmetric to the helix axis, but also give expressions for helical fields and fields parallel to the helix axis (like those related to an applied bias or the molecular dipole moment). Investigating these different field configurations allows us to determine which types of spin-orbit coupling terms can occur in this kind of geometry without using a fully general differential-geometric approach that might yield less transparent results.

The adiabatic theory is used to show that physically well-motivated approximations involving a separation ansatz are mathematically sound. In this regard, this work can be seen as

an application of an adapted version of the adiabatic approximation to derive an explicit physical model, which due to the inclusion of spin-orbit coupling lies beyond the range of applications of this theory discussed so far in the literature. Considering a greater variety of spin-orbit coupling terms makes it easier for us to determine whether the adiabatic approximation is applicable and how the existing approach has to be altered to do so. In particular, we find that the separation of the confinement and the spin-orbit inducing field is necessary to fulfill the requirements of the adiabatic method used here. Since our approach can be generalized to a broader class of geometrical set-ups, we intend to clear the way forward to the inclusion of spin-orbit coupling to the adiabatic description of confined quantum systems.

We also provide a classification of the terms in our effective Hamiltonian by applying unitary transformations and rewriting it in terms of an effective gauge and magnetic field. This allows for an easier comparison with other models and provides simple analytic expressions for the spin-related effective fields revealing their dependence on the model parameters. To round up our discussion, we also compute the spin polarization in the obtained effective model and show its dependence on various parameters.

II. THE MODEL

To describe an electron in 3D space with helical confinement and a generic spin-orbit coupling, we use the Pauli equation

$$H_{\mathbb{R}^3}\Psi = -\frac{\hbar^2}{2m}\Delta\Psi + V + \Phi - i\frac{\hbar^2}{4m^2c^2}\boldsymbol{\sigma} \cdot (\nabla\Phi \times \nabla\Psi). \quad (1)$$

with a confinement potential V and an additional scalar field Φ . The potential V rapidly increases in the directions normal to the helix (or some submanifold in general), thus restricting the particle motion to a small neighborhood of the helix, while the field Φ generates the spin-orbit coupling. The confinement can also be realized via homogeneous boundary conditions (which are equivalent to an infinitely deep potential well). $\boldsymbol{\sigma} = (\sigma_x, \sigma_y, \sigma_z)$ is the vector with the Pauli matrices as its entries and Ψ is a wave-function. The wave function Ψ takes values in spin space \mathbb{C}^2 (i. e. $\Psi \in L^2(\mathbb{R}^3, \mathbb{C}^2)$ which is the space of square integrable \mathbb{C}^2 -valued functions on 3-dimensional space).

The kinetic part of the Hamilton operator $H_{\text{kin},\mathbb{R}^3} = -\frac{\hbar^2}{2m}\Delta + V + \Phi$ is of Schrödinger type and is diagonal in spin space. The remaining part $H_{\text{SOC},\mathbb{R}^3}$ is referred to as the spin-orbit-

coupling (SOC) term. Notice that we are assuming that the confinement potential does not give rise to spin-orbit interaction terms; it just controls the extension of the electronic wave functions in the direction transversal to the helical path. The strength of the confinement is controlled by a confinement scale ε which the potential V depends on (see Sec. II C).

A. Adapted local coordinates

When dealing with a confined system we need to choose suitable coordinates that cover a sufficiently large neighborhood of the submanifold to which the particle motion is restricted. We consider a helix, which is 1-dimensional and can be described as an infinite Frenet curve \mathbf{c} in 3D space with constant curvature and torsion (see Fig. 1). Introducing local curvilinear coordinates, we obtain a map

$$\mathbf{r}(s, \rho, \varphi) := \mathbf{c}(s) + \rho \cos \varphi \mathbf{e}_2(s) + \rho \sin \varphi \mathbf{e}_3(s), \quad (2)$$

with

$$\begin{aligned} \mathbf{e}_2 &:= \cos \theta \mathbf{n} + \sin \theta \mathbf{b}, \\ \mathbf{e}_3 &:= -\sin \theta \mathbf{n} + \cos \theta \mathbf{b}, \end{aligned} \quad (3)$$

which represents a diffeomorphism from $\Omega_\varepsilon = \mathbb{R} \times (0, \varepsilon) \times (0, 2\pi)$ to the tubular neighborhood B_ε of \mathbf{c} for all $\varepsilon < 1/\kappa$. The first coordinate of the new system is simply the parameter of the curve \mathbf{c} , while ρ and φ are polar coordinates (with origin $\mathbf{c}(s)$) in the plane normal to $\mathbf{t}(s)$. This is the most convenient choice if the confinement potential is spherically symmetric in the normal directions. Note that the function $\theta(s)$ fixes a certain rotation of the planar coordinate axes around \mathbf{t} in each point s .

The metric tensor in these coordinates is given by:

$$g = \begin{pmatrix} (1 - \kappa\rho \cos(\varphi + \theta))^2 + \rho^2(\tau + \theta')^2 & 0 & \rho^2(\tau + \theta') \\ 0 & 1 & 0 \\ \rho^2(\tau + \theta') & 0 & \rho^2 \end{pmatrix} \quad (4)$$

and

$$\det g = \rho^2 (1 - \kappa\rho \cos(\varphi + \theta))^2. \quad (5)$$

We choose

$$\theta(s) = - \int_0^s \tau(\tilde{s}) d\tilde{s}, \quad (6)$$

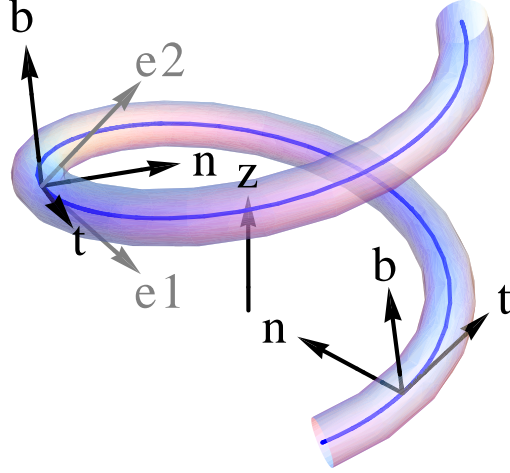


FIG. 1. Helix with surrounding tube, Frenet frame $\{\mathbf{t}, \mathbf{n}, \mathbf{b}\}$, rotated frame $\{\mathbf{t}, \mathbf{e}_1, \mathbf{e}_2\}$ and global z -axis.

which implies that the local frame $\left\{\frac{d\mathbf{r}}{ds}, \frac{d\mathbf{r}}{d\rho}, \frac{d\mathbf{r}}{d\varphi}\right\}$ is orthogonal on Ω_ϵ and g is a diagonal matrix. This choice is usually referred to as a Tang frame.

The map \mathbf{r} induces a transformation of the wave functions $A: L^2(B_\epsilon) \rightarrow L^2(\Omega_\epsilon)$ given by:

$$A\Psi := (\det g)^{1/4} \Psi \circ \mathbf{r}. \quad (7)$$

The transformation A is unitary and its inverse is:

$$A^\dagger\Psi = \left((\det g)^{-1/4} \Psi\right) \circ \mathbf{r}^{-1}. \quad (8)$$

The factor $(\det g)^{1/4}$ was introduced to absorb the volume element coming from the curvilinear coordinates.

B. The helix

An explicit unit speed parametrization for the helix can be given as:

$$\mathbf{c}(s) := \left(R \cos\left(\frac{2\pi s}{\tilde{R}}\right), R \sin\left(\frac{2\pi s}{\tilde{R}}\right), \frac{bs}{\tilde{R}}\right), \quad (9)$$

with

$$\tilde{R} := \pm\sqrt{(2\pi R)^2 + b^2}. \quad (10)$$

Using it, the corresponding Frenet frame reads:

$$\begin{aligned}
\mathbf{t}(s) &= \left(-\frac{2\pi R}{\tilde{R}} \sin\left(\frac{2\pi s}{\tilde{R}}\right), \frac{2\pi R}{\tilde{R}} \cos\left(\frac{2\pi s}{\tilde{R}}\right), \frac{b}{\tilde{R}} \right), \\
\mathbf{n}(s) &= \left(-\cos\left(\frac{2\pi s}{\tilde{R}}\right), -\sin\left(\frac{2\pi s}{\tilde{R}}\right), 0 \right), \\
\mathbf{b}(s) &= \left(\frac{b}{\tilde{R}} \sin\left(\frac{2\pi s}{\tilde{R}}\right), -\frac{b}{\tilde{R}} \cos\left(\frac{2\pi s}{\tilde{R}}\right), \frac{2\pi R}{\tilde{R}} \right).
\end{aligned} \tag{11}$$

The helix has constant curvature and torsion which are related to its radius R and pitch b by the expressions:

$$\kappa = \frac{4\pi^2 R}{\tilde{R}^2} \tag{12}$$

and

$$\tau = \pm \frac{b}{2\pi R} \kappa = \pm \frac{2\pi b}{\tilde{R}^2}. \tag{13}$$

It is worth noting that any curve with curvature and torsion both nonzero and constant is a (left- or right-handed) helix, so this parametrization describes all such curves. Therefore, the coordinates introduced in (2) with $\kappa, \tau = \text{const} \neq 0$ are called helical coordinates. Both b and \tilde{R} change signs when the helicity is reversed (i. e. the helix is replaced by its mirrored counterpart).

Furthermore, the following abbreviations will be used later on:

$$\mathbf{u}_\perp(s, \rho, \varphi) := \rho \cos(\varphi + \theta(s)) \mathbf{n}(s) + \rho \sin(\varphi + \theta(s)) \mathbf{b}(s) \tag{14}$$

which denotes all vectors orthogonal to the tangent vector $\mathbf{t}(s)$. As a result, the local parametrization becomes $\mathbf{x} = \mathbf{c} + \mathbf{u}_\perp$, while

$$\hat{n} = \mathbf{n} \cdot \mathbf{u}_\perp = \rho \cos(\varphi + \theta(s)), \quad \hat{b} = \mathbf{b} \cdot \mathbf{u}_\perp = \rho \sin(\varphi + \theta(s)) \tag{15}$$

are the projections of these normal vectors onto the Frenet frame.

C. Confinement potential

The confinement potential V in (1) restricts the particle motion to the proximity of the curve c . In curvilinear coordinates we have:

$$(AVA^\dagger)(s, \rho, \phi) = V(\mathbf{r}(s, \rho, \varphi)) = \varepsilon^{-2} V_0(s, \varepsilon^{-1} \rho, \varphi). \tag{16}$$

Assuming that the shape of the potential does not vary along the curve and that the potential is spherically symmetric, $V \circ \mathbf{r}$ only depends on ρ and the scaling factor ε which controls the strength of the confinement. If V is spherically symmetric, this can be imagined as the radius of a tube to which the electron motion is confined. As ε becomes small, the confinement increases while the tube radius shrinks. We require that V tends to $+\infty$ for $\rho \rightarrow \varepsilon$, which implies that the wave functions obey homogeneous Dirichlet boundary conditions.⁵⁵ This requirement is met by the potential well with walls of infinite height and radius ε . This potential is zero within the tube and thus realized by simply imposing the aforementioned boundary conditions on the wave functions. The tube radius ε is also our confinement scale, so the limit of strong confinement is equivalent to the tube having a radius close to zero. Mathematically $H_{\mathbb{R}^3}$ can be defined as the Friedrichs extension⁵⁶ of the operator in Eq. (1) defined on $C_c^\infty(B_\varepsilon)$. The form domain of the extension is $D(\sqrt{H_{\mathbb{R}^3}}) = H_0^1(B_\varepsilon)$.

So instead of a harmonic confinement as in Ref.³⁷ we use boundary conditions that are equivalent to an infinite-height two-dimensional potential well in the normal plane of each point of the helix. This potential has the advantage of being globally defined and also the accessible space is covered by one single coordinate patch.

We also define rescaled operators by

$$Q^\varepsilon := D_\varepsilon^\dagger \varepsilon^2 Q D_\varepsilon \quad (17)$$

with $(D_\varepsilon \Psi)(s, \rho, \varphi) := \varepsilon^{-1} \Psi(s, \varepsilon^{-1} \rho, \varphi)$. The transformation (17) corresponds to switching to microscopic time units $\tilde{t} = \varepsilon^{-2} t$ while at the same time rescaling V_0 to become independent of ε which means we have homogeneous boundary conditions on the cylinder Ω_1 with radius 1 instead of Ω_ε .

III. THE EFFECTIVE HAMILTONIAN

A. Transformation to helical coordinates

As we have seen in Sec. II A, the adapted local coordinates which are appropriate to describe our geometry are helical coordinates which give rise to the unitary transformation A as defined in Eq. (7). The relation between the Hamiltonian in euclidean and curvilinear

(helical) coordinates is

$$H_{\mathbb{R}^3} A^\dagger \Psi = A^\dagger H_{\text{curv}} \Psi \quad (18)$$

for $\Psi \in C_c^\infty(\Omega_\varepsilon)$ which extends to the entire domain of H_{curv} due to the uniqueness property of the Friedrichs extension (see Sec. III in the supplementary information).

We now rewrite the Hamilton operator (1) using the curvilinear coordinates (2). We start with the kinetic energy term in the Tang frame and obtain the following expression after applying the scaling transformation from Eq. (17):

$$H_{\text{kin,c}}^\varepsilon = -\frac{\hbar^2}{2m} \left(\frac{\partial^2}{\partial \rho^2} + \frac{1}{\rho^2} \frac{\partial^2}{\partial \varphi^2} + \frac{1}{(1 - \kappa \varepsilon \hat{n})^2} \varepsilon^2 \frac{\partial^2}{\partial s^2} + \frac{2\hat{b}\kappa\tau}{(1 - \kappa \varepsilon \hat{n})^3} \varepsilon^3 \frac{\partial}{\partial s} \right. \\ \left. + \frac{\varepsilon^2 \kappa^2}{4(1 - \kappa \varepsilon \hat{n})^2} + \frac{\kappa \tau^2 \varepsilon^3 (5\varepsilon \hat{b}^2 \kappa - 2\hat{n}(1 - \kappa \varepsilon \hat{n}))}{4(1 - \kappa \varepsilon \hat{n})^4} \right) \quad (19)$$

$H_{\text{kin,c}}^\varepsilon$ can be written as the sum of a longitudinal part $H_{\text{kin,l}}^\varepsilon$ and a transversal part $H_{\text{kin,t}}$ with the latter being

$$H_{\text{kin,t}} = -\frac{\hbar^2}{2m} \left(\frac{\partial^2}{\partial \rho^2} + \frac{1}{\rho^2} \frac{\partial^2}{\partial \varphi^2} + \frac{1}{4\rho^2} \right), \quad (20)$$

which is independent of ε . The longitudinal part of $H_{\text{kin,c}}^\varepsilon$ now only depends on partial derivatives with respect to the arc length s . Outside of $H_{\text{kin,t}}$, partial derivatives with respect to the transverse coordinates ρ and φ still appear in the spin-orbit coupling term $H_{\text{SOC,c}}$.

We assumed homogeneous boundary conditions for the tube B_ε , which is transformed and rescaled to the cylinder $\Omega_1 = \mathbb{R} \times B_2(0,1)$ (in cylinder coordinates). Therefore $H_{\text{kin,t}}$ is proportional to the 2-dimensional Dirichlet-Laplace operator $-\Delta$ on the 2d-ball $B_2(0,1)$ with radius 1. Later we will also explicitly write down $H_{\text{SOC,c}}$, the spin-orbit coupling term in helical coordinates.

For the following two sections we assume initial conditions Ψ_0 with $\|\Psi_0\| = 1$ and $\|\varepsilon^2 \Delta \Psi_0\|^2 \leq C$ which is sufficient to show adiabatic approximation. In Section III E we will restrict ourselves to initial conditions with $\|\varepsilon^2 \Delta \Psi_0\|^2 \leq C\varepsilon^2$ in order to obtain a simplified formula for the approximate Hamiltonian allowing for its direct computation using H_{curv} .⁵⁷ Furthermore, the Taylor expansion of $H_{\text{curv}}^\varepsilon$ up to second order in ε shall be denoted by

$$H^\varepsilon = H_{\text{kin}}^\varepsilon + H_{\text{SOC}}^\varepsilon = H_0 + \varepsilon H_1 + \varepsilon^2 H_2. \quad (21)$$

We observe that for states $\Psi \in \chi_{(-\infty, E]}(H^\varepsilon) L^2(\Omega_\delta)$, which is the subspace with energy cut-off at E , the Taylor expansion H^ε of $H_{\text{curv}}^\varepsilon$ differs from $H_{\text{curv}}^\varepsilon$ itself only by an error of order 3:

$$\|(H_{\text{curv}}^\varepsilon - H^\varepsilon) \Psi\|_{D(H^\varepsilon)} \leq \tilde{C} \varepsilon^3. \quad (22)$$

That this approximation is also valid for the time evolution generated by $H_{\text{curv}}^\varepsilon$ and H^ε can be shown by transferring the arguments in the proof of Ref.⁴⁶ (Corollary 1) to our situation.⁵⁸ Therefore, we can use the second order Taylor expansion H^ε of $H_{\text{curv}}^\varepsilon$ instead of the full expression.

B. Transversal solutions

We shall now determine the eigenfunctions of the transverse Hamiltonian $H_{\text{kin},t}$, together with the boundary condition which requires the solutions to vanish on the boundary of the unit circle (after the rescaling (17)). Those are required to calculate the effective (approximate) Hamiltonian below. Being a Dirichlet-Laplacian, $H_{\text{kin},t}$ has a purely discrete spectrum,⁵⁶ implying that all eigenenergies are isolated points. Since the transverse part does not depend on spin, we omit spin-degrees of freedom in this section entirely, thus dealing with complex-valued wave functions.

Using the ansatz

$$\psi_{N,l}(\rho, \varphi) = \sqrt{k_{N,|l|} \rho} J_{|l|}(k_{N,|l|} \rho) e^{il\varphi} \quad (23)$$

with $k_{N,|l|} = \frac{\sqrt{2mE_{N,|l|}}}{\hbar}$, we obtain for $x = k_{N,|l|} \rho$:

$$x^2 J_{|l|}''(x) + x J_{|l|}'(x) + (x^2 - l^2) J_{|l|}(x) = 0, \quad (24)$$

i. e., the $J_{|l|}$ are solution's of Bessel's differential equation. Since ψ has to be square integrable, the solutions $J_{|l|}$ are Bessel functions of the first kind. The energy $E_{N,|l|}$ is determined by the boundary condition $J_{|l|}(k_{N,|l|}) = 0$ to

$$E_{N,|l|} = \frac{\hbar^2}{2m} (j_{|l|,N})^2 \quad (25)$$

where $j_{|l|,N}$ is the N -th zero of the Bessel function $J_{|l|}$. l is an integer due to the periodicity of $\psi_{N,l}$ while $J_{|l|}$ only depends on the absolute value of l . The quantum number l labels the angular momentum part of the full wave function. The lowest energy with $l \neq 0$ is $E_{1,1}$ with

eigenstates $\psi_{1,1}$ and $\psi_{1,-1}$. The projection to the subspace of the $L^2(\Omega_1)$ -functions with the transverse part lying in the eigenspace of $E_{1,1}$ is defined as:

$$P_0 := \text{id} \otimes |\psi_{1,1}\rangle \langle \psi_{1,1}| + \text{id} \otimes |\psi_{1,-1}\rangle \langle \psi_{1,-1}|. \quad (26)$$

We also define a map $U_0: L^2(\Omega_\delta) \rightarrow L^2(\mathbb{R}, \mathbb{C}^2)$ whose restriction to $P_0 L^2(\Omega_\delta)$ is unitary, by:

$$(U_0 \Psi)_l(s) := \int_0^\delta \int_0^{2\pi} \psi_{1,l}^*(\rho, \varphi) \Psi(s, \rho, \varphi) \, d\varphi \, d\rho, \quad (27)$$

with the adjoint

$$\left(U_0^\dagger f \right)(s, \rho, \varphi) = \sum_{l \in \{-1, 1\}} \psi_{1,l}(\rho, \varphi) f_l(s). \quad (28)$$

This operator obeys the relations $U_0 U_0^\dagger = \text{id}$ and $U_0^\dagger U_0 = P_0$. Note that the subspace which U_0 maps into is $L^2(\mathbb{R}, \mathbb{C}^2)$, the space of square-integrable functions on the real line with values in \mathbb{C}^2 which does not describe spin (which is omitted here) but angular momentum orientation. So if we include spin again, we are dealing with $\mathbb{C}^2 \times \mathbb{C}^2$ -valued functions, which have both a spin and an angular momentum index.

C. Adiabatic approximation

We now aim at finding an approximation for the Hamiltonian $H_{\text{curv}}^\varepsilon$ in the limit of a strong confinement potential. The potential V_0 in Eq. (16) scales the directions normal to the helix by ε^{-1} , so that the confinement becomes strong for small ε . This means the potential well we use for confinement has radius ε and becomes arbitrarily narrow if ε goes to zero. This limit has structural similarities to the Born-Oppenheimer approximation with the transversal scaling factor ε taking the role of the electron to nucleus mass ratio. Therefore, ideas from adiabatic perturbation theory can be taken over to the case of strong confining forces.

We are looking for an effective Hamiltonian which is defined on the reduced space $U_0 L^2(\Omega_1, \mathbb{C}^2) = L^2(\mathbb{R}, \mathbb{C}^2 \times \mathbb{C}^2)$. Based on our previous considerations, an educated guess would be

$$H_{\text{eff}}^{(0)} = U_0 H^\varepsilon U_0^\dagger. \quad (29)$$

Indeed, for vanishing curvature and torsion and without spin-orbit coupling the $H_{\mathbb{R}^3}$ can be written as a sum of a purely transversal and a purely longitudinal contribution, allowing for

a simple separation ansatz. In other words $[H_{\mathbb{R}^3}, P_0] = 0$ would hold and

$$\left(U_0^\dagger H_{\text{eff}}^{(0)} U_0 - H_{\mathbb{R}^3} \right) P_0 = 0 \quad (30)$$

would follow. However, both the SOC term and the curved geometry spoil this simple behaviour and Eq. (30) is no longer true in general. Therefore, a careful estimate for the error introduced by replacing $H_{\text{curv}}^\varepsilon$ with some effective Hamiltonian is needed. In the following we sketch a way to get such an estimate using adiabatic perturbation theory.

Following the approach in Ref.⁴⁶ one starts by constructing a closed subspace of $L^2(\Omega_1)$ which is invariant up to some small error under the dynamics generated by H^ε . We call the orthogonal projector associated with this subspace P_ε and require the properties:⁵⁹

1. P_ε is bounded on $D((H^\varepsilon)^m)$ and $P_\varepsilon - P_0 = \mathcal{O}(\varepsilon)$ as a bounded operator on $D((H^\varepsilon)^m)$,
2. $[H^\varepsilon, P_\varepsilon] = \mathcal{O}(\varepsilon)$ as a bounded operator from $D((H^\varepsilon)^{m+1})$ to $D((H^\varepsilon)^m)$ and
3. $[H^\varepsilon, P_\varepsilon] \chi_{(-\infty, E]}(H^\varepsilon) = \mathcal{O}(\varepsilon^3)$ as a bounded operator from $L^2(\Omega_1)$ to $D((H^\varepsilon)^m)$.

The construction of P_ε is sketched in Sec. IV of the supplementary information.

By setting

$$U^\varepsilon := (P_0 P_\varepsilon + P_0^\perp P_\varepsilon^\perp) (\text{id} - (P_\varepsilon - P_0)^2)^{-1/2} \quad (31)$$

we obtain a unitary map $U^\varepsilon: L^2(\Omega_1) \rightarrow L^2(\Omega_1)$ whose restriction to $P_\varepsilon L^2(\Omega_1)$ is also unitary as a map from $P_\varepsilon L^2(\Omega_1)$ to $P_0 L^2(\Omega_1)$. U^ε is bounded as an operator on $D((H^\varepsilon)^m)$ and admits an expansion

$$U^\varepsilon = \text{id} + \varepsilon U_1^\varepsilon + \varepsilon^2 U_2^\varepsilon \quad (32)$$

with the U_i^ε being of order ε^0 (as operators on $D((H^\varepsilon)^m)$) and $P_0 U_1^\varepsilon P_0 = 0$ and $U_2^\varepsilon P_0 = P_0 U_2^\varepsilon P_0 = P_0 U_2^\varepsilon$.

Using U_0 and U^ε we define an operator $U := U_0 U^\varepsilon$ with the properties:

1. U is a unitary map from $P_\varepsilon \mathcal{H}$ to $L^2(\mathbb{R}^d, \mathbb{C}^2 \times \mathbb{C}^2)$,
2. $U U^\dagger = \text{id}_{L^2(\mathbb{R}^d)}$ and $U^\dagger U = P_\varepsilon$.

Setting $\tilde{H}_{\text{eff}} = U H^\varepsilon U^\dagger$ we can show that

$$\left\| \left(e^{-itH^\varepsilon} - U^\dagger e^{-it\tilde{H}_{\text{eff}}} U \right) P_\varepsilon \chi_{(-\infty, E]}(H^\varepsilon) \right\| \leq C_1 \varepsilon^3 (1 + |t|) \quad (33)$$

i. e. on the subspace $P_\varepsilon L^2(\Omega_1)$ with cut-off energy E , H^ε and H_{eff} yield approximately the same dynamics up to an error of order ε^3 (and up to an error of ε on the macroscopic time scale or times of order $\varepsilon^{-2}t$ respectively). This error estimate which follows from property 3. of P_ε by Duhamel's principle as in Ref.⁴⁶ (Eq. (31)) is our main technical result. It shows that the deviation between the time evolution of the effective and the full Hamiltonian is controlled by the adiabatic scale. This approximation is sometimes called a superadiabatic^{46,60} since the estimate depends on a power of ε greater than one. Likewise $\exp(-it\tilde{H}^\varepsilon)$ and $P_\varepsilon L^2(\Omega_1)$ are called superadiabatic evolution and subspace respectively. Estimates like (33) can be obtained without this super-adiabatic construction but with a power of ε below 3 which is insufficient for approximation on macroscopic time scales (see Ref.⁴⁶ (Sec. 1.2)).

While Eq. (33) gives us an error estimate for the adiabatic approximation, the effective Hamiltonian still differs from the guess we made in (29), which is more straightforward to calculate. However since U^ε is a second order polynomial in ε by (32), an additional argument similar to Ref.⁴⁶ (p. 52ff.) yields that we can neglect all higher order terms in (33) and $\tilde{H}_{\text{eff}} = U_0 U^\varepsilon H^\varepsilon (U^\varepsilon)^\dagger U_0^\dagger$ except for the expression

$$H_{\text{corr}} = \varepsilon^2 U_0 H_1 B_e H_1 U_0^\dagger \quad (34)$$

with $B_e = (E_0 - H_{\text{kin},t}^\perp)^{-1} P_0^\perp$ and $H_{\text{kin},t}^\perp$ being the restriction of $H_{\text{kin},t}$ to $P_0^\perp L^2(\Omega_1)$:

We can show

$$\left\| \left(\tilde{H}_{\text{eff}} - H_{\text{eff}} \right) \chi_{(-\infty, E]} \left(\tilde{H}_{\text{eff}} \right) \right\| \leq C_2 \varepsilon^3 \quad (35)$$

with

$$H_{\text{eff}} = H_{\text{eff}}^{(0)} + H_{\text{corr}}. \quad (36)$$

As in Ref.⁴⁶ (Corollary 2, see also p. 44) we can additionally replace U by U_0 in (33) while only acquiring an additional time-independent error of order ε to obtain⁶¹

$$\left\| \left(e^{-itH^\varepsilon} - U_0^\dagger e^{-itH_{\text{eff}}} U_0 \right) U_0^\dagger \chi_{(-\infty, E]} (H_{\text{eff}}) U_0 \right\| \leq C_3 \varepsilon (1 + \varepsilon^2 |t|) \quad (37)$$

with $H_{\text{eff}} = H_{\text{eff}}^{(0)} + H_{\text{corr}}$ as in (36). One might ask why those higher order terms were required in the first place. The answer is that we needed $[H^\varepsilon, P_\varepsilon] \chi_{(-\infty, E]} (H^\varepsilon) = \mathcal{O}(\varepsilon^3)$ to get the third order error estimate in (33). Using P_0 instead of P_ε together with $H_{\text{eff}}^{(0)} = U_0 H^\varepsilon U_0^\dagger$ would only give an error estimate of order ε because of $[H^\varepsilon, P_0] = \mathcal{O}(\varepsilon)$ due to the spin-orbit coupling terms and the higher order kinetic terms coming from the helical geometry.

We will now explicitly write down the kinetic part of $H_{\text{eff}}^{(0)}$. The scalar product $\langle \psi_{1,l} | H^\varepsilon \psi_{1,l'} \rangle$ involves integrations over φ and ρ . Because $\psi_{1,l'}$ is an eigenvector of $-i\frac{\partial}{\partial\varphi}$, the latter is always replaced by l' . From our calculation of H_{curv} , we now know that the prefactors of the derivatives are rational functions of \hat{b} and \hat{n} (see Eq. (19)). So $H_{\text{eff}}^{(0)}$ consists of expressions of the form

$$\int_0^\delta \int_0^{2\pi} \psi_{1,l}^*(\rho, \varphi) \rho^{k+n+m} \cos^n \varphi \sin^m \varphi \frac{\partial^r}{\partial \rho^r} \psi_{1,l'}(\rho, \varphi) d\varphi d\rho \quad (38)$$

multiplied with functions of s and partial derivatives with respect to s . Due to (15) and the φ -dependence of $\psi_{1,l}$, (38) vanishes for uneven values $n + m$ because of $l \in \{-1, 1\}$ and the orthogonality of the eigenfunctions. In the following, we therefore neglect terms with an uneven number of Sine and Cosine because these vanish upon projection anyway and therefore do not contribute to $H_{\text{eff}}^{(0)}$. So by taking the Taylor expansion of $H_{\text{kin},c}^\varepsilon$ and omitting uneven powers of the trigonometric functions, we obtain for the kinetic term:

$$H_{\text{kin}}^\varepsilon = -\frac{\hbar^2 \varepsilon^2}{2m} \left(\frac{\partial^2}{\partial s^2} + \frac{\kappa^2}{4} \left(1 + 3\rho^2 \varepsilon^2 (\ell_- + \ell_+ + 2) \frac{\partial^2}{\partial s^2} \right) \right) + H_{\text{kin},t} \quad (39)$$

where the definitions

$$\ell_+ := \exp(i2\varphi) \quad \text{and} \quad \ell_- := \exp(-i2\varphi) \quad (40)$$

were used.

D. Spin-orbit coupling

We assume that the spin-orbit coupling is induced by a scalar potential $\tilde{\Phi}$ leading to a radial field around the (global) x^3 -axis, i. e.

$$\tilde{\Phi}(\mathbf{x}) = \Phi \left(\sqrt{(x^1)^2 + (x^2)^2} \right). \quad (41)$$

As for $H_{\text{kin}}^\varepsilon$, the spin-orbit coupling term $H_{\text{SOC}}^\varepsilon$ is obtained by calculating the Taylor expansion of the full expression for the SOC up to second order in ε . We again omit uneven powers of Sine and Cosine because they vanish upon projection anyway. Using again the definition (40) this results in:

$$H_{\text{SOC}}^\varepsilon = \frac{\hbar^2 \varepsilon^2}{16m^2 c^2} \left(\Phi'(R) h_{01} + \Phi''(R) h_{02} \right) \quad (42)$$

with

$$\begin{aligned}
h_{01} = & 4\boldsymbol{\sigma} \cdot \mathbf{b}i \frac{\partial}{\partial s} \\
& + \left(\frac{b^2 \boldsymbol{\sigma} \cdot \mathbf{t} (\ell_- - \ell_+)}{R\tilde{R}^2} + \boldsymbol{\sigma} \cdot \mathbf{b}\tau (\ell_- - \ell_+) - i\boldsymbol{\sigma} \cdot \mathbf{n}\tau (\ell_- + \ell_+ - 2) \right) \rho \frac{\partial}{\partial \rho} \\
& + \left(\frac{b^2 \boldsymbol{\sigma} \cdot \mathbf{t} (\ell_- + \ell_+ - 2)}{R\tilde{R}^2} + \boldsymbol{\sigma} \cdot \mathbf{b}\tau (\ell_- + \ell_+ - 2) + i\boldsymbol{\sigma} \cdot \mathbf{n}\tau (\ell_+ - \ell_-) \right) \left(-i \frac{\partial}{\partial \varphi} \right) \\
& + \frac{b^2 \boldsymbol{\sigma} \cdot \mathbf{t} (\ell_+ - \ell_-)}{2R\tilde{R}^2} + \frac{1}{2} \boldsymbol{\sigma} \cdot \mathbf{b}\tau (\ell_+ - \ell_-) + \frac{1}{2} i\boldsymbol{\sigma} \cdot \mathbf{n}\tau (\ell_- + \ell_+ - 2)
\end{aligned} \tag{43}$$

and

$$h_{02} = \boldsymbol{\sigma} \cdot \mathbf{t} (\ell_+ - \ell_-) \rho \frac{\partial}{\partial \rho} - \boldsymbol{\sigma} \cdot \mathbf{t} (\ell_- + \ell_+ + 2) \left(-i \frac{\partial}{\partial \varphi} \right) + \frac{1}{2} \boldsymbol{\sigma} \cdot \mathbf{t} (\ell_- - \ell_+). \tag{44}$$

Since the full SOC Hamiltonian is self-adjoint, this series expansion is self-adjoint as well, which can also be checked by direct computation.

It is instructive to consider potentials with different symmetries as well. If we choose

$$\tilde{\Phi}(\mathbf{x}) = -E_z x^3 \tag{45}$$

i. e. a constant external field parallel to the global x^3 -axis which could be the result of a molecular dipole moment or an applied bias, we obtain

$$\begin{aligned}
H_{\text{SOC}}^\varepsilon = & \frac{i\hbar^2 \varepsilon^2}{2m^2 c^2} E_z \left(\frac{\pi R}{\tilde{R}} \left(\sigma_x \cos \left(\frac{2\pi s}{\tilde{R}} \right) + \sigma_y \sin \left(\frac{2\pi s}{\tilde{R}} \right) \right) \frac{\partial}{\partial s} \right. \\
& \left. + \frac{\pi^2 R}{\tilde{R}^2} \left(-\sigma_x \sin \left(\frac{2\pi s}{\tilde{R}} \right) + \sigma_y \cos \left(\frac{2\pi s}{\tilde{R}} \right) \right) \right)
\end{aligned} \tag{46}$$

which reproduces the result from Ref.²⁸ (Eq. (2)).

Another example is a field which is radially symmetric to the helix, i. e. it only depends on the normal distance parameter ρ :

$$\tilde{\Phi}(\mathbf{x}) = \Phi(\rho). \tag{47}$$

In this case the spin-orbit coupling reads

$$H_{\text{SOC}}^\varepsilon = \frac{\hbar^2}{4m^2 c^2} \left(-\Phi''(0) \varepsilon^2 \boldsymbol{l}\boldsymbol{\sigma} \cdot \mathbf{t} + \Phi'(0) \left(-\frac{\boldsymbol{l}\boldsymbol{\sigma} \cdot \mathbf{t}}{\rho} - \frac{1}{2} i\varepsilon^3 \kappa \rho \boldsymbol{\sigma} \cdot \mathbf{b} \frac{\partial}{\partial s} \right) \right). \tag{48}$$

This expression differs from (42) and (46) in that terms occur at different orders of ε . In case of $\Phi'(0) = 0$ the SOC term is of the same form ($\propto \boldsymbol{l}\boldsymbol{\sigma} \cdot \mathbf{t}$) as in Ref.³⁷ where the helical confinement potential acted as the source of the SOC.

s -dependent versions of all these fields can be considered as well; this leads to additional terms proportional to σ_x as well as s -dependent prefactors. Expressions for s -dependent fields are given in Sec. V of the supplementary information.

Had we used the confinement potential as the source for SOC as in Ref.³⁷, we would have run into an issue here: in this case $\Phi(\rho) = \frac{\hbar^2}{2m} \frac{\rho^2}{\varepsilon^4}$ would hold and therefore

$$- \frac{\hbar^4}{4m^3 c^2 \varepsilon^2} l \boldsymbol{\sigma} \cdot \mathbf{t} \quad (49)$$

would be the leading order term in $H_{\text{SOC}}^\varepsilon$. This is a contribution of order ε^{-2} which does not fit into the adiabatic approach presented here. Since the term becomes arbitrarily large for small ε it will be difficult to include it in any systematic approximation procedure dealing with the limit $\varepsilon \rightarrow 0$.

E. Projection with transversal states

We write down the particular cases of (38) that we need to calculate the effective Hamiltonian

$$H_{\text{eff}}^{(0)} = H_{\text{kin,e}} + H_{\text{SOC,e}}:$$

$$\begin{aligned} \int_0^{2\pi} \int_0^1 \psi_{1,l}^*(\rho, \varphi) \psi_{1,l'}(\rho, \varphi) \, d\rho \, d\varphi &= \delta_{ll'}, \\ \int_0^{2\pi} \int_0^1 \psi_{1,l}^*(\rho, \varphi) \rho \frac{\partial}{\partial \rho} \psi_{1,l'}(\rho, \varphi) \, d\rho \, d\varphi &= -\frac{1}{2} \delta_{ll'}, \\ \int_0^{2\pi} \int_0^1 \psi_{1,l}^*(\rho, \varphi) \rho^2 \psi_{1,l'}(\rho, \varphi) \, d\rho \, d\varphi &= \frac{1}{3} \end{aligned} \quad (50)$$

for $l \in \{-1, 1\}$.

Using these integrals we obtain

$$\begin{aligned} (H_{\text{kin,e}})_{ll'} &= E_{1,1} - \frac{\hbar^2 \varepsilon^2}{2m} \left(\left(\frac{\partial^2}{\partial s^2} - \frac{\kappa^2}{4} \left(2\varepsilon^2 \frac{\partial^2}{\partial s^2} + 1 \right) \right) \delta_{ll'} \right. \\ &\quad \left. - \frac{\varepsilon^2 \kappa^2}{4} \frac{\partial^2}{\partial s^2} (\delta_{ll'-2} + \delta_{ll'+2}) \right) \end{aligned} \quad (51)$$

and

$$(H_{\text{SOC},e})_{ll'} = \frac{\hbar^2 \varepsilon^2}{8m^2 c^2} \left(\Phi'(R) \left(-\frac{b^2 l \boldsymbol{\sigma} \cdot \mathbf{t}}{R \tilde{R}^2} + \boldsymbol{\sigma} \cdot \mathbf{b} (-l\tau + 2i \frac{\partial}{\partial s}) - i \boldsymbol{\sigma} \cdot \mathbf{n} \tau \right) + \Phi''(R) (-l \boldsymbol{\sigma} \cdot \mathbf{t}) \right) \delta_{ll'}. \quad (52)$$

For $\Phi'(R) = 0$ (e.g. if the radial field has a minimum at the radius of the helix) we again obtain an SOC term proportional to $-l \boldsymbol{\sigma} \cdot \mathbf{t}$ as in Ref.³⁷

At this point we note that unlike $H_{\text{SOC},e}$, $H_{\text{kin},e}$ is not proportional to $\delta_{ll'}$. However we can get rid of the off-diagonal term by using a more restricted initial condition. So instead of an initial state Ψ_0 with $\left\| \varepsilon^2 \frac{\partial^2 \Psi_0}{\partial s^2} \right\| \leq C$ we shall use a state with $\left\| \varepsilon^2 \frac{\partial^2 \Psi_0}{\partial s^2} \right\| \leq C \varepsilon^2$ from now on,⁶² i.e. the kinetic energy of Ψ_0 is of order ε^2 instead of ε^0 . The off-diagonal term will then be of order ε^4 and can therefore be neglected (see Eq. (22)).

We still have to address how to deal with the second term H_{corr} in (36). It depends on the resolvent map $(E_0 - H_{\text{kin},t}^\perp)^{-1}$ and the first order part H_1 of the Hamiltonian which reads:

$$H_1 = -\frac{\hbar^2}{m} \kappa \rho \cos \phi \varepsilon^2 \frac{\partial^2}{\partial s^2} + \frac{\hbar^2}{4m^2 c^2} \Phi'(R) i \left(\boldsymbol{\sigma} \cdot \mathbf{t} \left(\frac{\sin \phi}{2\rho} - \sin \phi \frac{\partial}{\partial \rho} - \frac{\cos \phi}{\rho} \frac{\partial}{\partial \varphi} \right) + \boldsymbol{\sigma} \cdot \mathbf{b} \varepsilon \frac{\partial}{\partial s} \right). \quad (53)$$

With our updated initial condition we can neglect all the terms coming from H_{corr} involving partial derivatives. The only remaining term is the one quadratic in the spin-orbit coupling constant $\frac{\hbar^2}{4m^2 c^2} \Phi'(R)$, which is a negligibly small correction to the first order spin-orbit coupling. The remainder of H_{eff} is now of the form (29), i.e. the second order Taylor expansion of the Hamiltonian in helical coordinates projected with the transversal states. Finally, the potential Φ which was included for consistency in Eq. (1) is up to second order in ε just the constant $\Phi(R)$, which leads to a trivial energy shift upon projection. The remaining kinetic and SOC terms are of second order in ε and we can simply divide them by ε^2 to switch back to the macroscopic time scale, thus getting an effective Hamiltonian completely independent of the scaling and also diagonal in l -space.

As mentioned before, the effective Hamiltonian acts on $\mathbb{C}^2 \times \mathbb{C}^2$ -valued wave functions (including spin); in other words the wave functions carry a (transversal) angular momentum and a spin index. However, our effective Hamiltonian is diagonal w.r.t. angular momentum. Therefore the reduced space $U_0 L^2(\Omega_1, \mathbb{C}^2) = L^2(\mathbb{R}, \mathbb{C}^2 \times \mathbb{C}^2)$ decomposes into two orthogonal sub-spaces, the eigenspaces of $-i\partial_\varphi$. In the following we will take advantage of

this by fixing a certain initial value for l (1 or -1 in our case) since no transition between the values can occur in our approximation, i.e. we fix l in Eq. (27) thereby getting an effective Hamiltonian depending on l as a parameter. Note that time reversal symmetry transforms this Hamiltonian into its $-l$ counterpart. This means that a certain choice of l , which is equivalent to restricting the Hamiltonian to the corresponding eigenspace, violates time-reversal symmetry.

We stress that this compact result can only be obtained with the revised initial conditions introduced above. Had we instead used an initial state with kinetic energies of order 1 (which was our first choice in Section III A) not only would the first term in Eq. (53) contribute to H_{corr} , but also the terms off-diagonal in l -space would no longer be small. As a result, we could no longer switch to macroscopic times by simply dividing by ε^2 , because the first term in (51) would be of order ε^{-2} afterwards. Also we could not separate the l and $-l$ states due to the off-diagonal terms in H_{eff} . While this situation is fully covered by our perturbation scheme, the resulting effective Hamiltonian would be much more complicated and contain different orders in ε as well as terms allowing transitions from l to $-l$.

F. Structure of the effective hamiltonian

Although H_{eff} can be expressed solely by invariants like $\boldsymbol{\sigma} \cdot \mathbf{t}$ and geometrical parameters, it is not obvious how the different terms influence spin transport. We can make the structure of H_{eff} more transparent by applying a unitary transformation³⁷

$$U_1(s) = \exp\left(i\sigma_z \frac{\pi s}{\tilde{R}}\right) = \begin{pmatrix} e^{i\vartheta(s)} & 0 \\ 0 & e^{-i\vartheta(s)} \end{pmatrix} \quad (54)$$

($\vartheta(s) := \pi s / \tilde{R}$).

This will not only allow us to write the Hamiltonian in an even more compact way but also yield s -independent pre-factors, allowing us to determine the electronic band structure using Fourier transformation. With the identities

$$U_1(-i) \frac{\partial}{\partial s} U_1^\dagger = -i \left(\frac{\partial}{\partial s} - i \frac{\pi}{\tilde{R}} \sigma_z \right), \quad (55)$$

$$U_1\left(-\frac{\partial^2}{\partial s^2}\right) U_1^\dagger = -\left(\frac{\partial^2}{\partial s^2} - 2i \frac{\pi}{\tilde{R}} \sigma_z \frac{\partial}{\partial s} - \frac{\pi^2}{\tilde{R}^2} \right), \quad (56)$$

$$\boldsymbol{\sigma} \cdot \mathbf{b} = \frac{b}{\tilde{R}} S + \frac{2\pi R}{\tilde{R}} \sigma_z, \quad \boldsymbol{\sigma} \cdot \mathbf{n} = -iS\sigma_z, \quad \boldsymbol{\sigma} \cdot \mathbf{t} = -\frac{2\pi R}{\tilde{R}} S + \frac{b}{\tilde{R}} \sigma_z, \quad (57)$$

and

$$S = \begin{pmatrix} 0 & ie^{-i2\vartheta} \\ -ie^{i2\vartheta} & 0 \end{pmatrix} = -U_1^\dagger \sigma_y U_1 \quad (58)$$

we get

$$\begin{aligned} UH_{\text{kin,e}}U^\dagger &= E_{1,1} - \frac{\hbar^2}{2m} \left(\frac{\partial}{\partial s} - i\frac{\pi}{\tilde{R}} \sigma_z \right)^2 \\ &= E_{1,1} + \frac{\hbar^2}{2m} \left(-\frac{\partial^2}{\partial s^2} + \frac{2\pi i}{\tilde{R}} \sigma_z \frac{\partial}{\partial s} + \frac{\pi^2}{\tilde{R}^2} \right) \end{aligned} \quad (59)$$

as well as

$$\begin{aligned} UH_{\text{SOC,e}}U^\dagger &= \frac{\hbar^2}{4m^2c^2} \left(\Phi' \left(\sigma_y \left(-i\frac{b}{\tilde{R}} \frac{\partial}{\partial s} - l\frac{4\pi^3 R^2}{\tilde{R}^3} \right) \right. \right. \\ &\quad \left. \left. + \sigma_z \left(i\frac{2\pi R}{\tilde{R}} \frac{\partial}{\partial s} - lb\frac{8\pi^2 R^2 + b^2}{2R\tilde{R}^3} \right) + \frac{2\pi^2 R}{\tilde{R}^2} \right) \right. \\ &\quad \left. + \Phi'' l \left(-\sigma_y \frac{\pi R}{\tilde{R}} - \sigma_z \frac{b}{2\tilde{R}} \right) \right). \end{aligned} \quad (60)$$

We now rewrite $UH_{\text{eff}}U^\dagger$ in terms of effective fields:

$$\begin{aligned} H_t = UH_{\text{eff}}U^\dagger &= E_{1,1} + -r\frac{\partial^2}{\partial s^2} + v \\ &\quad + \lambda \left(i2(\sigma_y A_y + \sigma_z A_z) \frac{\partial}{\partial s} + \sigma_y l B_y + \sigma_z l B_z \right). \end{aligned} \quad (61)$$

and redistribute terms to obtain

$$\begin{aligned} H_t &= E_{1,1} + r \left(-\left(\frac{\partial}{\partial s} - \frac{i\lambda}{r} \hat{A} \right)^2 - \frac{|\mathbf{A}|^2}{16m^2c^4} \right) + v \\ &\quad + \lambda \boldsymbol{\sigma} \cdot \mathbf{B}. \end{aligned} \quad (62)$$

Here we introduced the parameters

$$v = r\frac{2\pi^2 b^2}{\tilde{R}^4} + \lambda\Phi' \frac{4\pi^2 R}{\tilde{R}^2}, \quad (63)$$

$$r = \frac{\hbar^2}{2m}, \quad \lambda = \frac{\hbar^2}{8m^2c^2} \quad (64)$$

and the fields $\hat{A} = \boldsymbol{\sigma} \cdot \mathbf{A}$, $\mathbf{A} = (A_x, A_y, A_z)$ and $\mathbf{B} = (B_x, B_y, B_z)$ with components

$$A_x = 0, \quad A_y = -\Phi' \frac{b}{\tilde{R}}, \quad A_z = \Phi' \frac{2\pi R}{\tilde{R}} + \frac{r}{\lambda} \frac{\pi}{\tilde{R}}, \quad (65)$$

$$B_x = 0, \quad B_y = -\Phi'' \frac{2\pi R}{\tilde{R}}, \quad B_z = -\Phi' \frac{b}{R\tilde{R}} - \Phi'' \frac{b}{\tilde{R}}.$$

The transformed Hamiltonian consists of a kinetic term including a non-abelian gauge field \widehat{A} and a Zeeman-like term with an effective magnetic field \mathbf{B} . Since the derivatives $\Phi^{(n)}(R)$ are position-independent, \mathbf{A} and \mathbf{B} are constant vectors. Eq. (62) resembles the Pauli equation but there are important differences: the gauge field \widehat{A} is matrix-valued and thus the associated symmetry group is non-abelian. Also unlike an actual vector potential and associated magnetic field, \widehat{A} and \mathbf{B} are not related to each other. Notice that the last term in Eq. (62) does not violate time-reversal symmetry, since time inversion corresponds to the replacement rules $l \rightarrow -l$ and $\boldsymbol{\sigma} \rightarrow -\boldsymbol{\sigma}$.

Taking the Fourier transform of $UH_{\text{eff}}U^\dagger$ we can calculate the electronic band structure of H_{eff} which is shown in Fig. 2. The B_z -component of the Zeeman term splits the $l = 1$ and $l = -1$ energy bands while the B_y -component opens a gap of width $\approx 2\Phi''\lambda$. Since B_z is small, the splitting is small as well, so the $l = 1$ and -1 bands lie close to each other. The band structure allows to analyze some symmetry-related properties of our model. First of all, changing the helicity means changing the sign of both the pitch b and the parameter \widetilde{R} which controls the direction in which the helix is traversed depending on s . However, the angular momentum l always points into the direction of \mathbf{t} and thus depends on helicity itself. This means that for opposite helicities, electrons with opposite l correspond to one another. Hence, in order to calculate the helicity dependence of spin-related effects, one has to compare the case with helicity $\text{hel} = 1$ and $l = 1$ to the case with $\text{hel} = -1$ and $l = -1$. Therefore in Fig. 2 both helicities are plotted, with the spin orientation indicated for $l = 1$ in the positive and $l = -1$ in the negative case.

Applying the gauge transformation

$$U_{\mathbf{g}}(s) = \exp\left(-i\frac{\lambda}{r}s\widehat{A}\right) \quad (66)$$

leads to the Hamiltonian

$$U_{\mathbf{g}}H_{\text{t}}U_{\mathbf{g}}^\dagger = E_{1,1} + r\left(-\frac{\partial^2}{\partial s^2} - \frac{\lambda^2}{4r^2}|\mathbf{A}|^2\right) + v + \lambda U_{\mathbf{g}}\boldsymbol{\sigma} \cdot \mathbf{B}U_{\mathbf{g}}^\dagger. \quad (67)$$

So if $\mathbf{B} = 0$, the result (67) is diagonal in spin space, i.e. the spin-orbit coupling can be removed entirely via the transformation (66). This is consistent with the fact that Rashba-like spin-orbit interaction terms in a one-dimensional quantum wire can always be removed using a unitary transformation.²⁰ Therefore, the Zeeman-like term is essential for our model to include spin-dependent effects. This term stems from the projection of

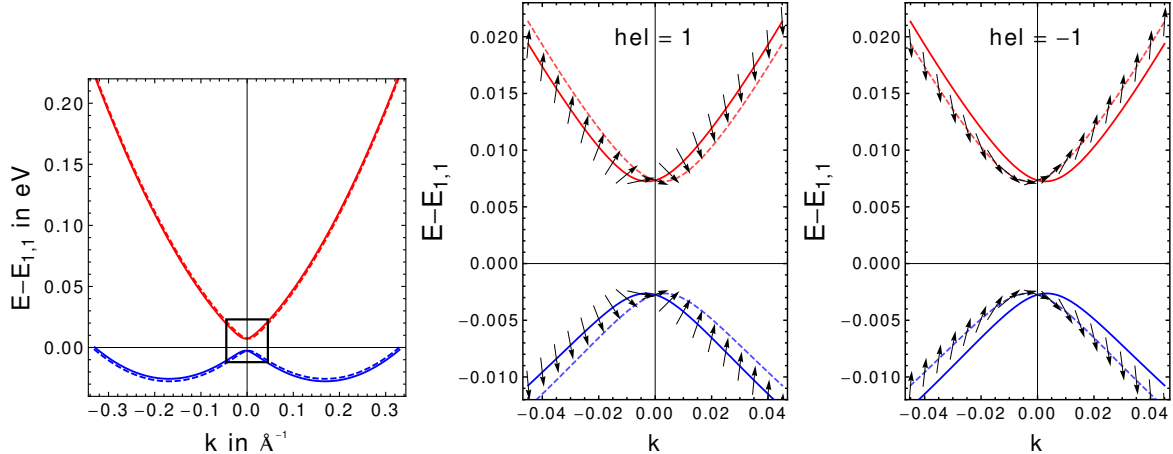


FIG. 2. Band structure for $R = 0.3 \text{ nm}$, $b = 0.3 \text{ nm}$, $r = 1 \text{ eV}\text{\AA}^2$ and $\Phi' = 0.005 \cdot \lambda^{-1} \text{ V/nm}$, $\Phi'' = 0.005 \cdot \lambda^{-1} \text{ V/nm}^2$. The second and third panel show an enhancement of the area around the gap as well as the spin orientations along the energy band belonging to $l = 1$ for positive ($\text{hel} = 1$) and $l = -1$ for negative ($\text{hel} = -1$) helicity. The solid lines belong to $l = 1$ while the dashed lines show the $l = -1$ energy band.

SOC contributions proportional to ∂_φ with the transversal states, leading to the transversal angular momentum l . The occurrence of the Zeeman term is therefore a direct result of the adiabatic approximation procedure. It is not present in models based on quantization,²⁸ or an approximation that neglects transversal states entirely,⁶³ but it appears in Ref.³⁷ since their effective Hamiltonian is calculated using rules similar to those we arrived at in Section III C. We note, however, that taking into account transversal operators as we do is not sufficient to obtain a model with a Zeeman term; it only occurs for certain field configurations. Indeed, the Hamiltonian (46) coincides with the quantization result and therefore only depends on the intrinsic geometry of the helix without retaining any information about the ambient space.

The Zeeman term is also remarkable since it does not involve momentum operators anymore (at least after choosing a certain l -eigenstate), thus yielding local (same-site) spin-orbit interactions after mapping on a discrete tight-binding Hamiltonian, as we shall see in the following section. Note that the gauge transformation (66) depends on λ/r which translates into the spin-orbit to electronic coupling ratio in the discrete case.

The transformed Hamiltonian also allows us to infer some of the dependence of spin-related effects on the model parameters. For example, looking at the expressions (65) we see that

in the case $\Phi'' = 0$ (e. g. for a field which is linear in the radial coordinate close to the helix radius R) these effects are very sensitive to the magnitude of the pitch. If on the other hand $\Phi' = 0$ while $\Phi'' \neq 0$ (e. g. if Φ has a local minimum at R), there is no gauge field \widehat{A} present at all and only the z -component of \mathbf{B} depends on the pitch. Even in the limit of a straight line which can be realized as $b \rightarrow 0$ and $R \rightarrow \infty$, the spin-dependence does not vanish since $B_y = -\Phi'' \neq 0$ remains.

G. The discretized Hamiltonian

Since we want to employ the Landauer formalism based on Green's function techniques to calculate spin transport, we map the continuum Hamiltonian obtained in the previous section on a more appropriate discrete tight-binding model. With the usual rules $\frac{\partial}{\partial s} \rightarrow \frac{1}{2a}(\delta_{kj-1} - \delta_{kj+1})$ and $\frac{\partial^2}{\partial s^2} \rightarrow \frac{1}{a^2}(\delta_{kj-1} + \delta_{kj+1} - 2\delta_{kj})$ we discretize the Hamiltonian:

$$H_t = E_{1,1} - r \frac{\partial^2}{\partial s^2} + v + \lambda \left(i\boldsymbol{\sigma} \cdot \mathbf{A} \frac{\partial}{\partial s} + l\boldsymbol{\sigma} \cdot \mathbf{B} \right) \quad (68)$$

from Eq. (62) to obtain:

$$\begin{aligned} H_{kj} &= (\varepsilon_0 + U_j) \delta_{kj} + t(\delta_{kj-1} + \delta_{kj+1}) \\ &+ i\lambda_1 \boldsymbol{\sigma} \cdot \mathbf{A} (\delta_{kj-1} - \delta_{kj+1}) + \lambda_2 l \boldsymbol{\sigma} \cdot \mathbf{B} \delta_{kj}, \end{aligned} \quad (69)$$

with

$$\varepsilon_0 = E_{1,1} + \frac{2r}{a^2} + v, \quad t = -\frac{r}{a^2}, \quad (70)$$

$$\lambda_1 = \frac{\lambda}{2a}, \quad \lambda_2 = \lambda. \quad (71)$$

a is the discretization parameter. In second quantization, Eq. (69) reads:

$$\begin{aligned} H &= (\varepsilon_0 + U_j) \sum_k \sum_{\sigma} d_{k,\sigma}^{\dagger} d_{k,\sigma} + t \sum_k \left(d_{k,\sigma}^{\dagger} d_{k+1,\sigma} + d_{k+1,\sigma}^{\dagger} d_{k,\sigma} \right) \\ &+ i\lambda_1 \sum_{k,\sigma,\sigma'} \left(d_{k,\sigma}^{\dagger} (\boldsymbol{\sigma} \cdot \mathbf{A})_{\sigma\sigma'} d_{k+1,\sigma'} - d_{k+1,\sigma}^{\dagger} (\boldsymbol{\sigma} \cdot \mathbf{A})_{\sigma\sigma'} d_{k,\sigma'} \right) \\ &+ \lambda_2 l \sum_k d_{k,\sigma}^{\dagger} (\boldsymbol{\sigma} \cdot \mathbf{B})_{\sigma\sigma'} d_{k,\sigma'}. \end{aligned} \quad (72)$$

Here, $d_{k,\sigma}$ annihilates a particle on lattice site k with spin σ . It is now apparent that the discretized version of the Zeeman term $\lambda_2 l \sum_k d_{k,\sigma}^{\dagger} (\boldsymbol{\sigma} \cdot \mathbf{B})_{\sigma\sigma'} d_{k,\sigma'}$ couples electrons with different spins at the same site as previously mentioned. Such a term is not present in the

hitherto considered phenomenological methods regardless of their respective origin with the exception of Ref.³⁷. This brings us to the conclusion that a carefully performed approximation can lead to substantially different results. Since we presented a way to derive our approximation scheme from basic quantum mechanical principles, we are confident that this additional term is not merely an artifact of the calculation but is physically justified, provided that the prerequisites for the application of our procedure are fulfilled in the applications. As the discussion after Eq. (67) already suggested, this term also has profound consequences regarding the occurrence of spin-polarization, which we will further discuss in the results section.

IV. TRANSPORT

To investigate the implications of the discretized model from Eq. (72) regarding the CISS effect, we calculate the transmission and polarization in the Landauer regime. The quantum mechanical transmission function in a two-terminal setup can be written as⁶⁴⁻⁶⁶

$$T = \text{tr} \left(\Gamma_L (G^r)^\dagger \Gamma_R G^r \right) \quad (73)$$

where

$$G^r(E) = (E\mathbf{1} - H_{\text{eff}} - \Sigma(E)) \quad (74)$$

is the retarded Green's function⁶⁴ of the isolated molecule with the total self energy $\Sigma(E) = \Sigma_L(E) + \Sigma_R(E)$ accounting for the coupling to the metallic electrodes and encoding both the strength of this coupling as well as the density of states in the electrodes. The spectral densities $\Gamma_{L,R}(E)$ are, as usual, defined in terms of the self-energies as $\Gamma_{L,R}(E) = i \left(\Sigma_{L,R} - \Sigma_{L,R}^\dagger \right)$. To simplify the calculations, we will assume in what follows the wide-band approximation, where the self-energies (and hence the spectral densities) are assumed to be purely imaginary, energy-independent quantities. We therefore obtain:

$$\Sigma_{L,R} = -\frac{i}{2} \Gamma_{L,R} \quad (75)$$

with

$$(\Gamma_{L,R})_{ij}(E) = \sum_{\mu} \tilde{\gamma}_{\mu} \delta_{i,i_{\mu}} \delta_{i_{\mu},j} \quad (76)$$

where $\tilde{\gamma}_{\mu}$ depends on the couplings between lead and molecule and the electronic coupling in the lead. So in this case the Γ 's are just diagonal matrices with all diagonal entries

either zero or equal to the coupling $\tilde{\gamma}_\mu$ of the lead attached to the corresponding site of the molecule.

Assuming that the leads are not spin-polarized, the spin-polarization can be obtained by calculating the current spin polarization vector^{65,67}

$$(P_x, P_y, P_z) = \mathbf{P} = \frac{\text{tr} \left(\Gamma_L (G^r)^\dagger \Gamma_R \boldsymbol{\sigma} G^r \right)}{\text{tr} \left(\Gamma_L (G^r)^\dagger \Gamma_R G^r \right)} \quad (77)$$

where $\boldsymbol{\sigma} = (\sigma_x, \sigma_y, \sigma_z)$ is the vector containing the Pauli matrices in the appropriate dimension, e. g.

$$\sigma_x = \begin{pmatrix} 0 & \mathbf{1}_{N \times N} \\ \mathbf{1}_{N \times N} & 0 \end{pmatrix}, \quad (78)$$

The z -component in particular reads

$$P_z = \frac{T_\uparrow - T_\downarrow}{T_\uparrow + T_\downarrow} \quad (79)$$

with $T_s = \text{tr} \left(\Gamma_L (G^r)^\dagger \Gamma_R \pi_s G^r \right)$ for $s = \uparrow, \downarrow$.

For spin-polarized incoming electrodes we use the transmission function

$$T^u = \text{tr} \left(\pi_\uparrow \Gamma_L (G^{r,u})^\dagger \Gamma_R G^{r,u} \right) \quad (80)$$

with $G^{r,u}(E) = (E\mathbf{1} - H_{\text{eff}} - \Sigma^u(E))$ and $\Sigma^u(E) = \pi_\uparrow \Sigma_L(E) + \Sigma_R(E)$ which describes a system with its left electrode totally polarized in the spin-up direction and the analogously defined transmission T^d for the spin-down case.

While T_\uparrow and T_\downarrow as used in Eq. (79) are just components of the full transmission for certain spin-channels, the transmissions T^u and T^d that appear in and after Eq. (80) refer to transmissions with one incoming spin-channel entirely disconnected from the molecule. We define the spin polarization for this scenario by

$$P = \frac{T^u - T^d}{T^u + T^d}. \quad (81)$$

Despite this equation looking almost the same as (79) it is not the expectation value of an observable of our model (like the z -component of the spin polarization vector as in Eq. (79)) but rather the normed difference of transmission functions for two copies of the system with different incoming lead configurations (totally up or down polarized). The quantity (81) is closely related to the polarization measured in transport experiments with polarized electrodes.^{2,6,68,69}

V. RESULTS

The transmission and polarization for the Hamiltonian (72) were calculated using two sets of geometrical parameters: one for DNA and one for Helicene as listed in Table I. Since we only have one characteristic electronic coupling t , we chose it to be 0.2 eV for DNA and of the order of 1 eV for helicene. The first value is roughly of the order of magnitude obtained in semi-empirical calculations of realistic DNA structures,⁷⁰ the second value is roughly half of the typical $\pi - \pi$ interaction in carbon-based systems. The value of the spin-orbit interaction was taken as 5 meV in both cases to have a common reference point. It is of the same order of magnitude as in our recent estimations for helicene based on a coarse-grained model.⁷¹ The specific values of these parameters have only a quantitative effect on our results. Since we have a single electronic state per site on the helix, the obtained electronic structure would display no gap; hence, we add a staggering potential $U_k = (-1)^k \Delta\varepsilon$ (with $\Delta\varepsilon = t/2$) to open a band gap mimicking the HOMO-LUMO gap in a molecule.

The results for different combinations of helicity and angular momentum for DNA are shown in Fig. 3. The polarization changes sign only if both helicity and angular momentum are reversed, which is not surprising in light of our statement on the correspondence of these quantities at the end of Sec. III E. Indeed, Fig. 3 shows that the spin polarization depends on the helicity if the corresponding angular momenta are considered. We note that the linear behavior of the polarization around $E = 0$ may be a spurious numerical effect related to calculating the ratio of two small quantities when computing the polarization. Since electrons with opposite angular momentum have opposite spin polarization, the model can only yield a non-vanishing polarization if the two angular momenta occur at unequal rates in the initial state because otherwise the two contributions would cancel out.

In Fig. 4 and Fig. 5 the energy-dependent spin polarizations for DNA and helicene parameters are shown for different choices of the electric field behavior.

In qualitative agreement with experimental results,^{69,72} the DNA model yields a substantially higher overall spin polarization. This is probably due to its favorable electronic to spin-orbit coupling ratio which enhances the contribution from the Zeeman term (see Eq. (67) and the discussion thereafter). The oscillatory energy dependence is however similar for both systems.

The polarizations depicted in Figures 3, 4 and 5 were calculated according to Eq. (79), i. e.

	DNA	Helicene		DNA	Helicene
t (eV)	0.2	1			
R (nm)	2.37	0.26	A_y	-0.445	-0.438
b (nm)	3.4	0.36	A_z	-2.163	-189.213
$\lambda_1 \Phi'$ (meV)	5	5	B_y	-1.366	-4.616
$\lambda_2 \Phi''$ (meV)	5	5	B_z	-0.406	-1.895
$r/\lambda = -t\lambda_2/(4\lambda_1^2)$ (eV)	-10	-50			

TABLE I. Parameters used for transport calculations (left), resulting fields (right, for both $\Phi' \neq 0$ and $\Phi'' \neq 0$).

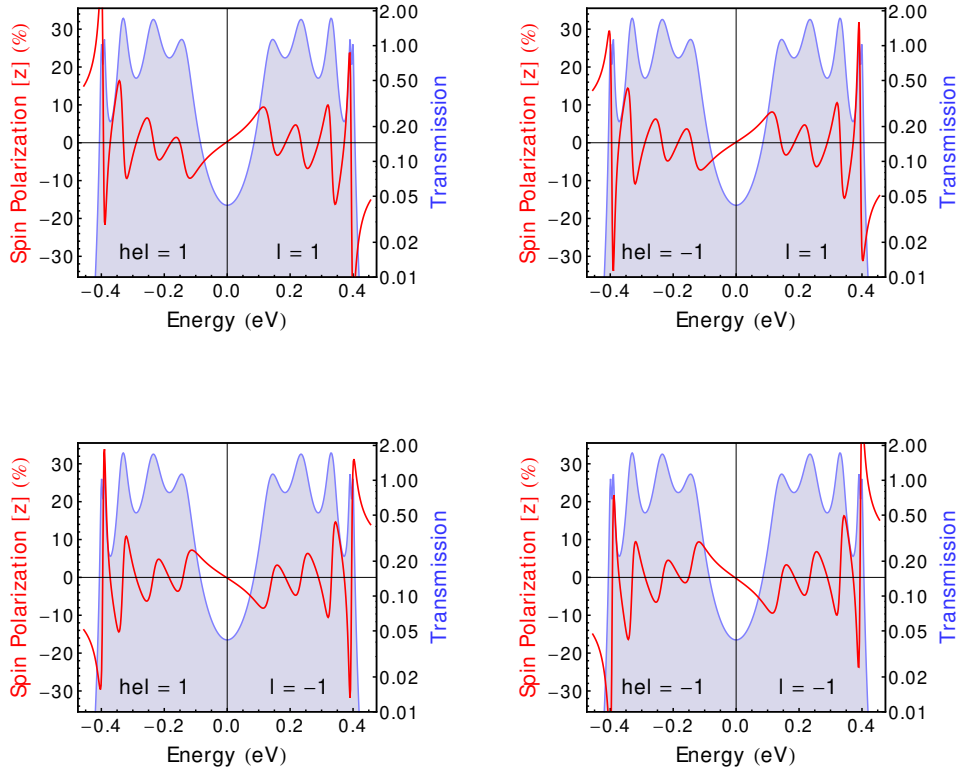


FIG. 3. Polarization P_z (unpolarized incoming leads, Eq. (79)) for different combinations of helicity hel and angular momentum l for DNA. To obtain opposite polarization, both the helicity hel of the molecule and the sign of the transversal angular momentum l have to be reversed. This is consistent with the fact that the angular momentum points into the direction of the tangent vector \mathbf{t} and therefore depends on the helicity.

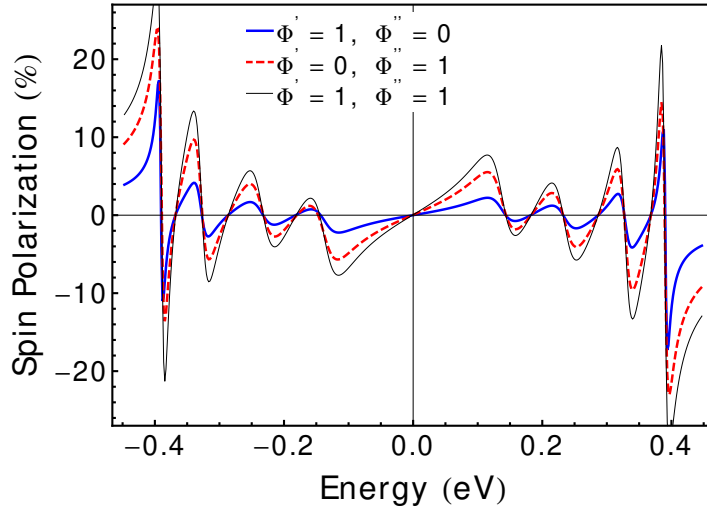


FIG. 4. Polarization P_z (unpolarized incoming leads, Eq. (79)) for different field configurations for DNA parameters.

for unpolarized incoming states. We did the same calculations using Eq. (81) and found only a negligible difference (less than 0.5%) between (79) and (81) for Helicene. For DNA there is a slightly larger deviation; yet comparing the result for Eq. (81) depicted in Fig. 6 with Fig. 4 shows overall similarity in magnitude and oscillatory behavior. This result shows that independently of the spin of the incoming state (which can be controlled by selecting the values of the coupling $\Gamma_{L,\uparrow}$ and $\Gamma_{L,\downarrow}$ for the corresponding incoming spin channels) the polarization has the same sign for most energies.

We remark that in this approach a finite spin polarization is obtained in the conductance of the system already for a single linear chain with a single electronic state per site. This is a consequence of the peculiar form of the spin-orbit interaction in Eq. (62), obtained after projecting the 3d problem on to the effective 1d model. This leads to the Zeeman-like term, which cannot be fully removed by any unitary transformation as previously discussed. Other models required more than one coupled chain with several in- and outgoing electrodes⁶³ or, alternatively a decoherence mechanism described as Büttiker probes^{20,31} to yield non-vanishing spin polarization. Relying on multiple coupled chains to prevent removal of the SOC also renders the results sensitive to electronic versus spin-orbit coupling ratios, which in cases like helicene can lead to very small polarization compared to experimental

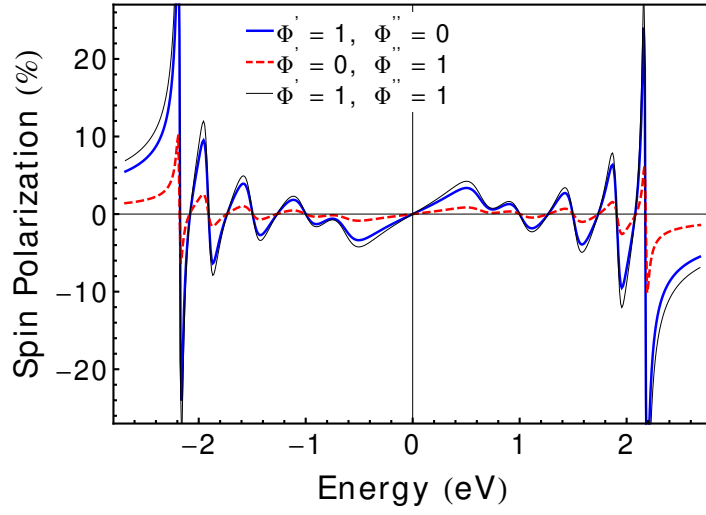


FIG. 5. Polarization P_z (unpolarized incoming leads, Eq. (79)) for different field configurations for helicene parameters. Overall polarization is smaller than in the DNA case, but the oscillatory behavior is similar.

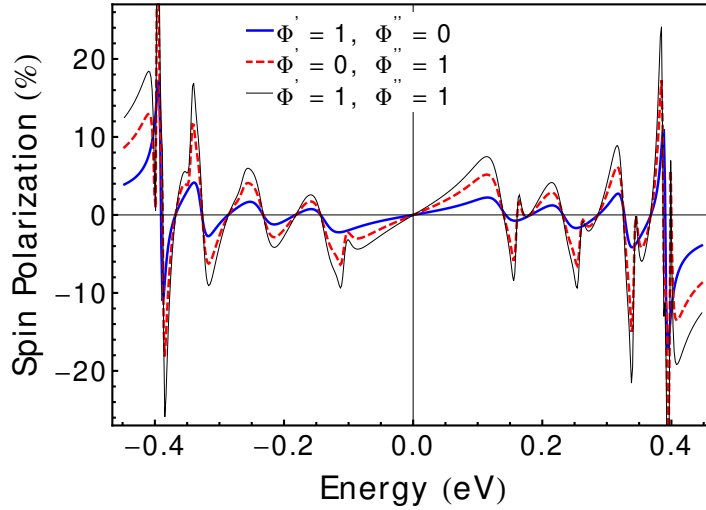


FIG. 6. Polarization P for polarized incoming leads (Eq. (81)) for different field configurations for DNA. Compared to the unpolarized case, the polarization is slightly enhanced in some regions (sometimes in the opposite direction) but the overall behavior and magnitude is similar.

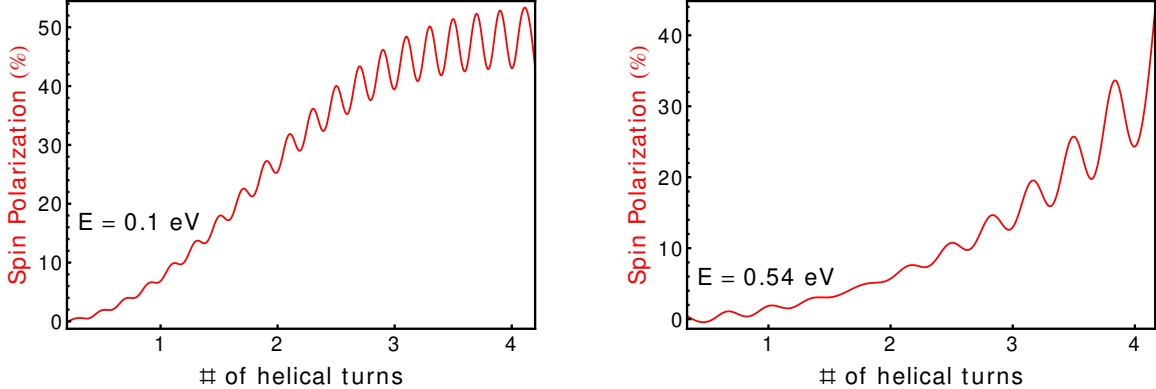


FIG. 7. Length dependence of the Polarization P_z (unpolarized incoming leads, Eq. (79)) for DNA (left) and helicene at energy E close to the band gap.

observations⁷¹.

We also investigate the dependence of the spin polarization on the molecule length. Assuming 10 lattice sites per helical turn for DNA and 6 for helicene we calculate the polarization at a fixed energy close to the gap depending on the number of helical turns in the molecule. The spin polarization increases with the length of the molecule with a roughly linear correlation despite oscillations as shown in Fig. 7 for DNA and helicene.

VI. CONCLUSIONS

We have derived a 1-dimensional effective model for electrons moving through a helical confinement. The model includes spin-orbit coupling coming from a generic scalar field to describe spin-dependent effects. We have applied a mathematically sound approximation procedure to show that the effective Hamiltonian follows from basic quantum mechanical principles in the limit of strong confinement. Since the adiabatic approximation theory we applied was developed for a far more general differential geometric setting (but without spin-dependent effects) it is likely that our approach can be carried out for a much wider class of systems including spin-dependent effects as well, starting from confinement to arbitrary curves to generic submanifolds. Restricting ourselves to the helical case we obtained a model suited to contribute to the description of the CISS effect. The model is similar in some respect to the one put forward in Ref.³⁷ with which it shares a momentum-independent

SOC term that does not occur in other models, and which is the result of the inclusion of transversal degrees of freedom during the approximation. This term prevents removal of the spin-orbit coupling using a gauge transformation as it is possible in 1-dimensional models lacking the term. One can thus expect non-zero polarization, as confirmed by our transport calculations in the linear transport regime. This sets this kind of models apart from others that require multiple incoming and outgoing transport channels or, alternatively, dephasing and decoherence effects to produce similar results. Being able to obtain similar terms in tight-binding models might therefore introduce sizeable spin polarization in a larger class of models.

The Pauli equation (1) with spin-orbit coupling we started with is already an approximation of the relativistic Dirac equation for energies which are small compared to the rest energy mc^2 . In this regard our effective Hamiltonian is the result of two subsequent limits: the non-relativistic limit and the adiabatic confinement. These limits are not interchangeable, which was recently pointed out by Shitade and Minamitani.⁷³ They showed that by taking the non-relativistic limit of the Dirac equation confined to a helix, a spin-orbit coupling of order $(mc^2)^{-1}$ coming from the confinement potential persists, while the usual SOC term in the Pauli equation is of order $(mc^2)^{-2}$. Clarifying the relation between these two approaches could help understanding the role of the different SOC terms contributing to the CISS effect.

SUPPLEMENTARY MATERIAL

The supplementary information contains a brief summary of the required tools from differential geometry, additional details on the adiabatic approximation as well as expressions for the spin-orbit coupling terms generated by s -dependent fields.

ACKNOWLEDGMENTS

The authors thank Karen Michaeli, Ron Naaman, Solmar Varela, Vladimiro Mujica, and Arezoo Dianat for very fruitful discussions. This work is funded by the European Union (ERDF) and the Free State of Saxony via the ESF projects 100231947 and 100339533 (Young Investigators Group “Computer Simulations for Materials Design – CoSiMa”). G.C. acknowledges financial support from the Volkswagen Stiftung (grant nos. 88366). This

work was partly supported by the German Research Foundation (DFG) within the Cluster of Excellence “Center for Advancing Electronics Dresden”. We acknowledge the Center for Information Services and High Performance Computing (ZIH) at TU Dresden for computational resources.

REFERENCES

- ¹D. Mishra, T. Z. Markus, R. Naaman, M. Kettner, B. Göhler, H. Zacharias, N. Friedman, M. Sheves, and C. Fontanesi, “Spin-Dependent Electron Transmission Through Bacteriorhodopsin Embedded in Purple Membrane,” *Proc. Nat. Acad. Sci. USA* **110**, 14872 (2013).
- ²V. Kiran, S. R. Cohen, and R. Naaman, “Structure Dependent Spin Selectivity in Electron Transport Through Oligopeptides,” *J. Chem. Phys.* **146**, 92302 (2017).
- ³P. C. Mondal, C. Fontanesi, D. H. Waldeck, and R. Naaman, “Field and Chirality Effects on Electrochemical Charge Transfer Rates: Spin Dependent Electrochemistry,” *ACS Nano* **9**, 3377 (2015).
- ⁴V. Kiran, S. P. Mathew, S. R. Cohen, I. Hernández Delgado, J. Lacour, and R. Naaman, “Helicenes – A New Class of Organic Spin Filter,” *Adv. Mat.* **28**, 1957 (2016).
- ⁵K. Michaeli, N. Kantor-Uriel, R. Naaman, and D. H. Waldeck, “The Electron’s Spin and Molecular Chirality – How are They Related and How do They Affect Life Processes?” *Chem. Soc. Rev.* **45**, 6478 (2016).
- ⁶A. C. Aragonès, E. Medina, M. Ferrer-Huerta, N. Gimeno, M. Teixidó, J. L. Palma, N. Tao, J. M. Ugalde, E. Giralt, I. Díez-Pérez, and V. Mujica, “Measuring the Spin-Polarization Power of a Single Chiral Molecule,” *Small* **13**, 1602519 (2017).
- ⁷A. Kumar, E. Capua, M. K. Kesharwani, J. M. L. Martin, E. Sitbon, D. H. Waldeck, and R. Naaman, “Chirality-Induced Spin Polarization Places Symmetry Constraints on Biomolecular Interactions,” *Proc. Nat. Acad. Sci. USA* **114**, 2474 (2017).
- ⁸M. Kettner, B. Göhler, H. Zacharias, D. Mishra, V. Kiran, R. Naaman, C. Fontanesi, D. H. Waldeck, S. Şek, J. Pawłowski, and J. Juhaniewicz, “Spin Filtering in Electron Transport Through Chiral Oligopeptides,” *J. Phys. Chem. C* **119**, 14542 (2015).
- ⁹R. Naaman and D. H. Waldeck, “Spintronics and Chirality: Spin Selectivity in Electron Transport Through Chiral Molecules,” *Annu. Rev. Phys. Chem.* **66**, 263 (2015).

- ¹⁰W. Mtangi, F. Tassinari, K. Vankayala, A. Vargas Jentzsch, B. Adelizzi, A. R. A. Palmans, C. Fontanesi, E. W. Meijer, and R. Naaman, “Control of Electrons’ Spin Eliminates Hydrogen Peroxide Formation During Water Splitting,” *J. Am. Chem. Soc.* **139**, 2794 (2017).
- ¹¹O. Ben Dor, S. Yochelis, A. Radko, K. Vankayala, E. Capua, A. Capua, S.-H. Yang, L. T. Baczewski, S. S. P. Parkin, R. Naaman, and Y. Paltiel, “Magnetization Switching in Ferromagnets by Adsorbed Chiral Molecules Without Current or External Magnetic Field,” *Nat. Commun.* **8**, 14567 (2017).
- ¹²T. J. Zwang, S. Hürlimann, M. G. Hill, and J. K. Barton, “Helix-Dependent Spin Filtering Through the DNA Duplex,” *J. Am. Chem. Soc.* **138**, 15551 (2016).
- ¹³M. Kettner, V. V. Maslyuk, D. Nürenberg, J. Seibel, R. Gutierrez, G. Cuniberti, K.-H. Ernst, and H. Zacharias, “Chirality-dependent electron spin filtering by molecular monolayers of helicenes,” *J. Phys. Chem. Lett.* **9**, 2025 (2018).
- ¹⁴J. M. Abendroth, K. M. Cheung, D. M. Stemer, M. S. El Hadri, C. Zhao, E. E. Fullerton, and P. S. Weiss, “Spin-dependent ionization of chiral molecular films,” *J. Am. Chem. Soc.* **141**, 3863–3874 (2019), <https://doi.org/10.1021/jacs.8b08421>.
- ¹⁵K. Ray, S. P. Ananthavel, D. H. Waldeck, and R. Naaman, “Asymmetric scattering of polarized electrons by organized organic films of chiral molecules,” *Science* **283**, 814 (1999).
- ¹⁶B. Göhler, V. Hamelbeck, T. Z. Markus, M. Kettner, G. F. Hanne, Z. Vager, R. Naaman, and H. Zacharias, “Spin Selectivity in Electron Transmission Through Self-Assembled Monolayers of Double-Stranded DNA,” *Science* **331**, 894 (2011).
- ¹⁷Z. Xie, T. Z. Markus, S. R. Cohen, Z. Vager, R. Gutiérrez, and R. Naaman, “Spin specific electron conduction through dna oligomers,” *Nano Lett.* **11**, 4652 (2011).
- ¹⁸S. Yeganeh, M. A. Ratner, E. Medina, and V. Mujica, “Chiral electron transport: Scattering through helical potentials,” *J. Chem. Phys.* **131**, 014707 (2009).
- ¹⁹R. Gutierrez, E. Díaz, R. Naaman, and G. Cuniberti, “Spin-selective transport through helical molecular systems,” *Phys. Rev. B* **85**, 081404 (2012).
- ²⁰A.-M. Guo and Q.-F. Sun, “Spin-selective transport of electrons in dna double helix,” *Phys. Rev. Lett.* **108**, 218102 (2012).
- ²¹E. Medina, F. López, M. A. Ratner, and V. Mujica, “Chiral molecular films as electron polarizers and polarization modulators,” *Europhys. Lett.* **99**, 17006 (2012).

- ²²R. Gutierrez, E. Díaz, C. Gaul, T. Brumme, F. Domínguez-Adame, and G. Cuniberti, “Modeling spin transport in helical fields: Derivation of an effective low-dimensional hamiltonian,” *J. Phys. Chem. C* **117**, 22276 (2013).
- ²³A. A. Eremko and V. M. Loktev, “Spin sensitive electron transmission through helical potentials,” *Phys. Rev. B* **88**, 165409 (2013).
- ²⁴D. Rai and M. Galperin, “Electrically driven spin currents in dna,” *J. Phys. Chem. C*. **117** (2013).
- ²⁵S. Varela, E. Medina, F. López, and V. Mujica, “Inelastic Electron Scattering from a Helical Potential: Transverse Polarization and the Structure Factor in the Single Scattering Approximation,” *J. Phys. Condens. Matter* **26**, 15008 (2014).
- ²⁶A.-M. Guo, E. Díaz, C. Gaul, R. Gutierrez, F. Domínguez-Adame, G. Cuniberti, and Q.-F. Sun, “Contact effects in spin transport along double-helical molecules,” *Phys. Rev. B* **89**, 205434 (2014).
- ²⁷A.-M. Guo and Q.-F. Sun, “Spin-dependent electron transport in protein-like single-helical molecules,” *Proc. Natl. Acad. Sci. USA* **111**, 11658 (2014).
- ²⁸E. Medina, L. A. González-Arraga, D. Finkelstein-Shapiro, B. Berche, and V. Mujica, “Continuum model for chiral induced spin selectivity in helical molecules,” *J. Chem. Phys.* **142**, 194308 (2015).
- ²⁹S. Matityahu, Y. Utsumi, A. Aharony, O. Entin-Wohlman, and C. A. Balseiro, “Spin-dependent transport through a chiral molecule in the presence of spin-orbit interaction and non-unitary effects,” *Phys. Rev. B* **93**, 75407 (2016), arXiv:1512.00793.
- ³⁰S. Behnia, S. Fathizadeh, and A. Akhshani, “Dna spintronics: Charge and spin dynamics in dna wires,” *J. Phys. Chem. C* **120**, 2973 (2016).
- ³¹S. Matityahu, Y. Utsumi, A. Aharony, O. Entin-Wohlman, and C. A. Balseiro, “Spin-dependent transport through a chiral molecule in the presence of spin-orbit interaction and nonunitary effects,” *Phys. Rev. B* **93**, 075407 (2016).
- ³²R. A. Caetano, “Spin-current and spin-splitting in helicoidal molecules due to spin-orbit coupling,” *Sci. Rep.* **6**, 23452 (2016).
- ³³E. Díaz, R. Gutiérrez, C. Gaul, G. Cuniberti, and F. Domínguez-Adame, “Coherent spin dynamics in a helical arrangement of molecular dipoles,” *AIMS Mater. Sci.* **4**, 1052 (2017).
- ³⁴H.-N. Wu, X. Wang, and W.-J. Gong, “Highly-polarized spin currents through protein-like single-helical molecules,” *Chem. Phys. Lett.* **677**, 131 (2017).

- ³⁵E. Díaz, P. Albares, P. G. Estévez, J. M. Cerveró, C. Gaul, E. Diez, and F. Domínguez-Adame, “Spin dynamics in helical molecules with nonlinear interactions,” *New J. Phys.* **20**, 043055 (2018).
- ³⁶S. Dalum and P. Hedegård, “Theory of chiral induced spin selectivity,” *Nano Letters* **19**, 5253–5259 (2019).
- ³⁷K. Michaeli and R. Naaman, “Origin of spin-dependent tunneling through chiral molecules,” *J. Phys. Chem. C* **123**, 17043–17048 (2019).
- ³⁸J. Fransson, “Chirality-induced spin selectivity: The role of electron correlations,” *J. Phys. Chem. Lett.* **10**, 7126 (2019).
- ³⁹V. V. Maslyuk, R. Gutierrez, A. Dianat, V. Mujica, and G. Cuniberti, “Enhanced magnetoresistance in chiral molecular junctions,” *J. Phys. Chem. Lett.* **9**, 5453–5459 (2018).
- ⁴⁰M. S. Zöllner, S. Varela, E. Medina, V. Mujica, and C. Herrmann, “Chiral-induced spin selectivity: A symmetry analysis of electronic transmission,” *ChemRxiv* (2019), <https://doi.org/10.26434/chemrxiv.8325248.v1>.
- ⁴¹S. Waldmann, *Poisson-Geometrie und Deformationsquantisierung: Eine Einführung* (Springer-Verlag, 2007) p. 612.
- ⁴²R. C. T. da Costa, “Quantum mechanics of a constrained particle,” *Phys. Rev. A* **23**, 1982–1987 (1981).
- ⁴³P. Maraner, “A complete perturbative expansion for quantum mechanics with constraints,” *J. Phys. A* **28**, 2939–2951 (1995).
- ⁴⁴K. A. Mitchell, “Gauge fields and extrapotentials in constrained quantum systems,” *Phys. Rev. A* **63**, 1–20 (2001).
- ⁴⁵R. Froese and I. Herbst, “Realizing holonomic constraints in classical and quantum mechanics,” *Commun. Math. Phys.* **220**, 489–535 (2001).
- ⁴⁶J. Wachsmuth and S. Teufel, “Effective Hamiltonians for Constrained Quantum Systems,” *Mem. Am. Math. Soc.* **230** (2014).
- ⁴⁷A. Martinez and V. Sordani, “On the Time-Dependent Born-Oppenheimer Approximation with Smooth Potential,” *Comptes Rendus Acad. Sci. Paris* **1**, 1–9 (2002).
- ⁴⁸V. Sordani, “Reduction Scheme for Semiclassical Operator-Valued Schrödinger Type Equation and Application to Scattering,” *Commun. Partial. Differ. Equ.* **28**, 1221–1236 (2003).
- ⁴⁹G. Panati, H. Spohn, and S. Teufel, “The time-dependent Born-Oppenheimer approximation,” *ESAIM: M2AN* (2007).

- ⁵⁰S. Teufel, *Adiabatic Perturbation Theory in Quantum Dynamics* (Springer Science & Business Media, 2003) p. 204.
- ⁵¹F. E. Meijer, A. F. Morpurgo, and T. M. Klapwijk, “One-dimensional ring in the presence of Rashba spin-orbit interaction: Derivation of the correct Hamiltonian,” *Phys. Rev. B* **66**, 033107 (2002).
- ⁵²E. Zhang, S. Zhang, and Q. Wang, “Quantum transport in a curved one-dimensional quantum wire with spin-orbit interactions,” *Phys. Rev. B* (2007).
- ⁵³J. Y. Chang, J. S. Wu, and C. R. Chang, “Exact hamiltonians with rashba and cubic dresselhaus spin-orbit couplings on a curved surface,” *Phys. Rev. B* **87**, 1–12 (2013).
- ⁵⁴C. Ortix, “Quantum mechanics of a spin-orbit coupled electron constrained to a space curve,” *Phys. Rev. B* **91**, 245412 (2015).
- ⁵⁵Provided the confinement potential $V(\mathbf{r}(s, \rho, \varphi)) = \varepsilon^{-2}V_0(s, \varepsilon^{-1}\rho, \varphi)$ is of order ε^{-4} (e. g. $V_0(\rho) = 1/(2\varepsilon^4)\rho^2$), this is in fact not a limitation: Ref.⁴⁵ (Prop. 8.1) shows that under the initial condition $\|\varepsilon^2\Delta\Psi_0\|^2 \leq C$ the time evolution of $H_{\mathbb{R}^3}$ approximates its counterpart with Dirichlet boundary conditions added.
- ⁵⁶E. B. Davies, *Spectral Theory and Differential Operators* (Cambridge University Press, 1995) p. 182.
- ⁵⁷Using $\|\varepsilon^2\Delta\Psi_0\|^2 \leq C\varepsilon^2$ instead of $\|\varepsilon^2\Delta\Psi_0\|^2 \leq C$ simplifies the adiabatic construction if no spin-orbit coupling terms are present. Including SOC however negates this advantage, so we might as well start with the more general condition and strengthen it at a later point if necessary.
- ⁵⁸Replace $H_{\mathcal{A}}^\varepsilon$ with $H_{\text{curv}}^\varepsilon$ and $H_{\text{eff}}^\varepsilon$ with \tilde{H}_{eff} and use Eq. (33).
- ⁵⁹Here and in the following, the domain $D(H)$ of an operator H is always assumed to be equipped with the graph norm. If H is closed, $D(H)$ is a Hilbert space whose scalar product induces the graph norm and $H \in \mathcal{L}(D(H), \mathcal{H})$ holds.
- ⁶⁰A. Joye and C. E. Pfister, “Superadiabatic evolution and adiabatic transition probability between two nondegenerate levels isolated in the spectrum,” *J. Math. Phys.* **34**, 454–479 (1993).
- ⁶¹Most of the proof carries over to our situation by replacing $H_{\text{eff}}^{(2)}$ with H_{eff} , $H_{\text{eff}}^\varepsilon$ with \tilde{H}_{eff} and U^ε with U . $U - U_0 = \mathcal{O}(\varepsilon)$ in $\mathcal{L}(L^2(\Omega_1), L^2(\mathbb{R}))$ follows directly from (32).
- ⁶²The initial condition introduced in Sec. III A allowed for kinetic energies of the same order as the confinement potential, see Eq. (16). With the revised initial condition, the kinetic

energy has to be small compared to the confinement thus narrowing the energy range where the approximation is justified.

- ⁶³R. Gutierrez, E. Díaz, C. Gaul, T. Brumme, F. Domínguez-Adame, and G. Cuniberti, “Modeling Spin Transport in Helical Fields: Derivation of an Effective Low-Dimensional Hamiltonian,” *J. Phys. Chem. C* **117**, 22276–22284 (2013).
- ⁶⁴S. Datta, *Electronic Transport in Mesoscopic Systems* (Cambridge University Press, 1995).
- ⁶⁵R. A. Bell, *Conduction in Carbon Nanotube Networks* (Springer, 2015).
- ⁶⁶M. Paulsson and M. Brandbyge, “Transmission eigenchannels from nonequilibrium Green’s functions,” *Phys. Rev. B* **76**, 1–7 (2007), 0702295.
- ⁶⁷B. K. Nikolić and S. Souma, “Decoherence of transported spin in multichannel spin-orbit-coupled spintronic devices: Scattering approach to spin-density matrix from the ballistic to the localized regime,” *Phys. Rev. B* **71**, 1–15 (2005), arXiv:0402662 [cond-mat].
- ⁶⁸P. C. Mondal, C. Fontanesi, D. H. Waldeck, and R. Naaman, “Field and chirality effects on electrochemical charge transfer rates: Spin dependent electrochemistry,” *ACS Nano* **9**, 3377 (2015).
- ⁶⁹V. K., S. P. Mathew, S. R. Cohen, I. Hernández Delgado, J. Lacour, and R. Naaman, “Helicenes—a new class of organic spin filter,” *Adv. Mat.* **28**, 1957 (2016).
- ⁷⁰T. Kubař, P. B. Woiczikowski, G. Cuniberti, and M. Elstner, “Efficient calculation of charge-transfer matrix elements for hole transfer in dna,” *J. Phys. Chem. B* **112**, 7937–7947 (2008).
- ⁷¹M. Geyer, R. Gutierrez, V. Mujica, and G. Cuniberti, “Chirality-Induced Spin Selectivity in a Coarse-Grained Tight-Binding Model for Helicene,” *J. Phys. Chem. C* **123**, 27230–27241 (2019).
- ⁷²B. Göhler, V. Hamelbeck, T. Z. Markus, M. Kettner, G. F. Hanne, Z. Vager, R. Naaman, and H. Zacharias, “Spin selectivity in electron transmission through self-assembled monolayers of double-stranded dna,” *Science* **331**, 894 (2011).
- ⁷³A. Shitade and E. Minamitani, “Geometric Spin-Orbit Coupling and Chirality-Induced Spin Selectivity,” arxiv.org (2020), arXiv:2002.05371.